Delayed and Sustained Remote Triggering of Small Earthquakes in the San Jacinto Fault Region by the 2014 Mw 7.2 Papanoa, Mexico Earthquake

Bo Li[1,2] (iD), Abhijit Ghosh[1] (iD), and Manuel M. Mendoza[1] (iD)

[1]Department of Earth Sciences, University of California, Riverside, CA, USA, [2]Department of Earth and Environmental Sciences, Ludwig-Maximilians University, Munich, Germany

Abstract We apply a move max matched-filter method to detect heightened seismicity triggered in the San Jacinto fault (SJF) zone, by the 2014 Mw 7.2 Papanoa, Mexico earthquake. The move max matched filter detects 5.4 and 1.7 times the number of earthquakes in the Southern California Seismic Network catalog and those detected by the matched-filter method, respectively. The seismicity rate increases significantly ~3.5 hr after the passage of the teleseismic waves and persists above the background level for about 1 week. This observation of delayed triggering may imply that dynamic stresses had initiated a time-dependent advance to failure or a secondary process. A highly active triggered patch is located ~10 km west of the SJF near Anza, on a previously unmapped fault. Focal mechanisms and a best fit plane suggest a normal fault perpendicular to the SJF. The unmapped fault may indicate higher seismic hazard in the surrounding areas if a large earthquake nucleated around the Anza seismic gap.

1. Introduction

With the implementation of globally distributed seismic networks and improved earthquake detection/location methods, large earthquakes have been widely observed to change the seismicity rate both dynamically (instantaneously) and in a delayed manner, within regions hundreds to thousands of kilometers away (Ghosh et al., 2009; Hill et al., 1993; Mendoza et al., 2016; Meng & Peng, 2014; Shelly et al., 2011). The dynamic stress changes due to large earthquakes at teleseismic distances have been estimated to be between 0.1 and 1 MPa (Prejean & Hill, 2009); thus, the occurrence of triggered earthquakes indicates that faults in that region are sensitive to small stress perturbations. For this reason, studies of triggered earthquakes provide clues to understanding the state of stress of critically stressed and potentially seismically hazardous faults (Johnson et al., 2015).

The San Jacinto Fault Zone (SJFZ) is currently the most seismically active fault segment in southern California (Hauksson et al., 2012; Kagan et al., 2006). It consists of several right-lateral strike-slip faults that have produced 11 earthquakes with magnitudes larger than 6 in the last 120 years (Bailey et al., 2010; Kagan et al., 2006). The central region of the SJFZ, a segment known as the Anza seismic gap, has not spawned a major earthquake for over 200 years (Rockwell et al., 1990). Previous studies show that there is a potential for an earthquake with magnitude 6.5 or larger to occur in this seismically quiet segment (Sanders & Kanamori, 1984; Thatcher et al., 1975). Therefore, understanding the stress state and the conditions required for rupture nucleation in the Anza gap or on neighboring faults is important for estimating the earthquake hazard in this area.

At 14:27:24 (UTC) on 18 April 2014, the Mw 7.2 Papanoa, Mexico earthquake occurred within the Guerrero seismic gap, as a result of thrust motion at shallow depth along the Cocos-North America plate boundary (Mendoza & Martínez López, 2017). The event resulted in unprecedented damage near the epicenter and minor damage in Mexico City. In this study, we build upon the commonly used template matched-filter method and apply the move max matched-filter (MMMF) method to detect seismic events in this region, 1 month before and after the Papanoa earthquake. A similar method has been applied previously by Shelly et al. (2007) to detect "weak" low-frequency earthquakes. We then use hypoinverse (Klein, 2002) and hypoDD (Waldhauser, 2001) to locate and relocate all detected events with high precision. Finally, we investigate the spatiotemporal distribution of relocated earthquakes, compare them to other earthquake catalogs, and discuss the possibility that these events were triggered and, if so, investigate the triggering mechanisms.

2. Data and Methods

In this study, we use continuous seismic data from 17 stations surrounding the San Jacinto fault (Figure 1) to detect and locate local earthquakes in the study region that were triggered by the 2014 Mw 7.2 Papanoa earthquake. The data spans 1 month before and 1 month after the Papanoa event. During this period, there are 880 local events recorded by the Southern California Seismic Network (SCSN) catalog (Figure 1). All events in this catalog are used as templates to perform the matched-filter and MMMF methods in detecting any local event missed (or undetected) by the network. For each catalog (template) event, we cut a 20-s time window (resampled at 20 samples per second) after the event origin time. Afterward, the template is used to perform a sliding time-window search throughout the 2- to 7-Hz band-passed data set, (with 0.05-s time steps) to detect other similar or correlated waveforms.

We first use the traditional template matched-filter method (Gibbons & Ringdal, 2006). This method is useful in developing larger catalogs, since it works on a well-tested assumption: If the template and matched waveform are highly correlated, the matched waveform represents an event that shares a similar location, station move-out, and focal mechanism as the template event. The method calculates the cross-correlation coefficients between the template event and the continuous waveforms in each of the three station-channel components, sums the coefficients across all stations, and retains newly detected events that met or exceed some predetermined, confidence threshold value. After experimenting with several thresholds by visually checking the seismograms of randomly selected events detected by the traditional template matched-filter method, we chose a uniform threshold value of 6 times the root mean square to detect new events in the 2-month data period.

One significant limitation of the traditional matched-filter method, though, is that any given template does not usually produce the maximum cross-correlation coefficient at the exact same move-out time in all stations for the missing events. Furthermore, for the same time step, some stations show peak coefficients, while others show much smaller or even negative coefficients, with peak coefficients a few time steps (0.05–1 s in our case) away, which lowers the summed coefficients under the threshold (supporting information Figure S1a). This is because even though some events are located close to the catalog events, their spatial offset is significant enough to result in different time lags across each station, relative to the template event. To reconcile this, Zhang and Wen (2015) developed the Match and Locate method to improve their detections by adding potential hypocentral locations on grid nodes around the template location. They then calculate the theoretical move-out at each potential location and time shift the seismic waveform accordingly before stacking and calculating the cross-correlation coefficients. The Match and Locate method can detect small events near the template location but may still miss events that lie in areas between the template location and the grid nodes. In addition, the velocity model used to compute the traveltime may be crude and result in an inaccurate move-out calculation. Furthermore, it is computationally inefficient to calculate the move-out for all the grid nodes to all the stations. The MMMF method — implemented with the SEC-C code (Senobari et al., 2018), we use in this study builds upon these traditional methods, yet overcomes their limitations. The first step of the MMMF method is similar to the traditional method by calculating the cross-coefficient for each station-channel component; however, instead of summing the cross-coefficients directly with constant move-out for each template, the MMMF method dynamically replaces the coefficient with the maximum coefficient 1 s before and after the current time step (Figures S1b and S1c). In other words, we allow discrepancies in the locations within a 1-s traveltime distance away from the template event. Our method then sums the move max coefficients and removes the mean values to make it comparable with the matched-filter results (Figure S1d). This method applies the same threshold used in the matched-filter method to obtain earthquake detections.

After obtaining a detection catalog, we use the cross-correlation between the template and the matched-event for each station to calculate P and S wave arrival times on the vertical and horizontal components, respectively. Lastly, we use a 1-D velocity model from Scott et al. (1994) to locate all detected P and S phases using hypoinverse (Klein, 2002) and then relatively relocate them with higher precision using hypoDD (Waldhauser, 2001).

3. Results

Local earthquakes in the San Jacinto fault region triggered by the Mw 7.2 Papanoa earthquake are shown in Figures 2b and 2c. These figures show a remarkable increase in microseismic activity after the Papanoa
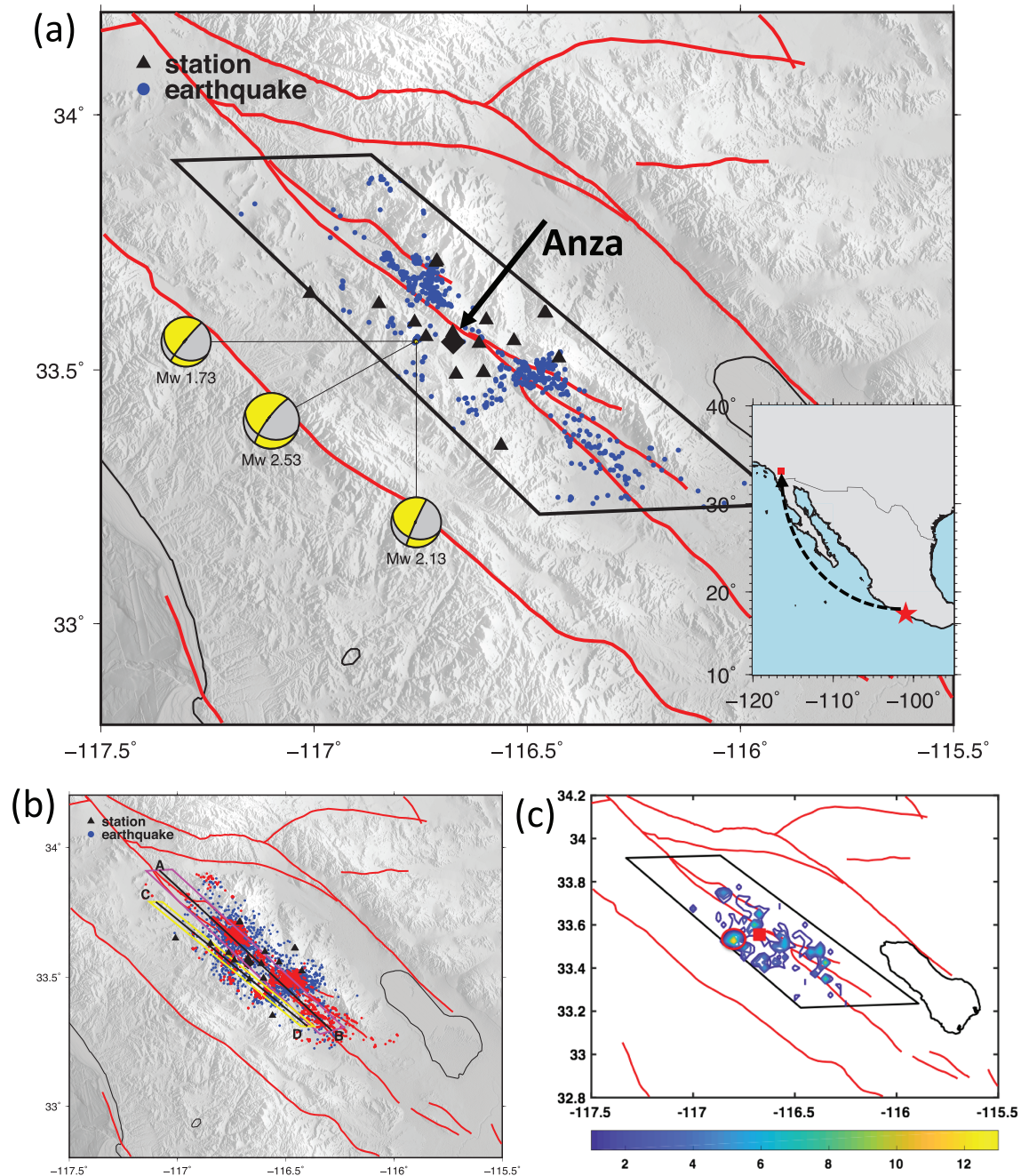
Figure 1. (a) Study region in southern California (black polygon). The red lines show the traces of mapped faults. Each blue dot represents one event in the Southern California Seismic Network catalog 30 days before and after the 2014 Mw 7.2 Papanoa, Mexico earthquake. Black triangles represent the seismic stations used in this study. Station information can be found in Table S1. The red star in the inset map shows the location of the Papanoa earthquake, while the red square marks the study area presented here. Three beach balls determined in this study show normal fault focal mechanisms in the off-fault earthquake cluster discussed in the main text. The black dashed arrow indicates the great circle travel path of the teleseismic (Papanoa) event to the study region. (b). Distribution of detected earthquakes. The blue dots represent earthquakes detected by the move max matched-filter method and located using hypoDD, while the red dots represent earthquakes from the Quake Template Matching catalog (Ross et al., 2019). The magenta and yellow polygons encompass the relocated earthquakes used to show the cross-section along Lines A–B in Figure S3 and C–D in Figure 4b. (c). Seismicity rate ratio plot (after and before the Mw 7.2 Papanoa earthquake). Since the cutoff here is selected to be 1, the colored region represents the area of seismicity rate increase. The red ellipse shows the most seismically active region that we interpreted to be triggered by the Papanoa earthquake. The red square marks the town of Anza, California.

earthquake, particularly, a few hours after the passage of the teleseismic wave train. This heightened seismic activity is also shown in a spectrogram and histogram (Figures 2c and 3a). Using the 880 catalog events in the 2-month data period as templates, the matched-filter and MMMF detect 2,835 and 4,765 local earthquakes
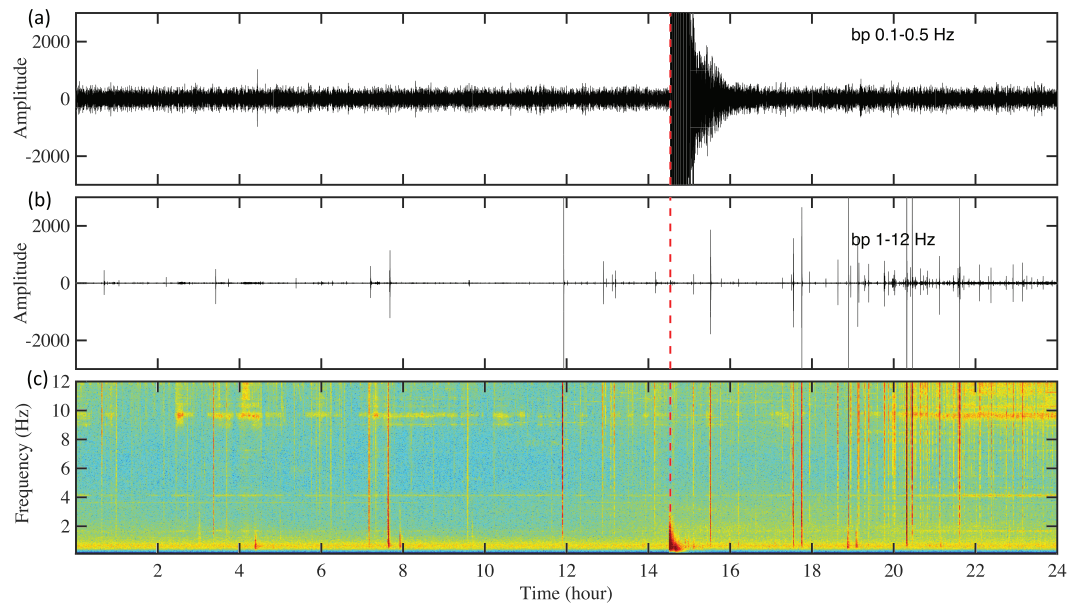
Figure 2. (a) One day seismogram filtered in 0.1- to 0.5-Hz band-pass to show the teleseismic signal of the Mw 7.2 Papanoa earthquake. (b) Same seismogram but filtered in 1–12 Hz to show local seismic signals. (c) Spectrogram (0.1–12 Hz) showing both local earthquakes and the Mw 7.2 Papanoa earthquake. The red dashed line marks the occurrence time of the teleseismic event.

— about 3.2 and 5.4 times the number of catalogued events, respectively (Figure 3a). These results show an elevated level of seismicity that lasts up to 7 days before returning to the background level. To better assess how the newly detected events compare with the original catalog events, we normalize the cumulative
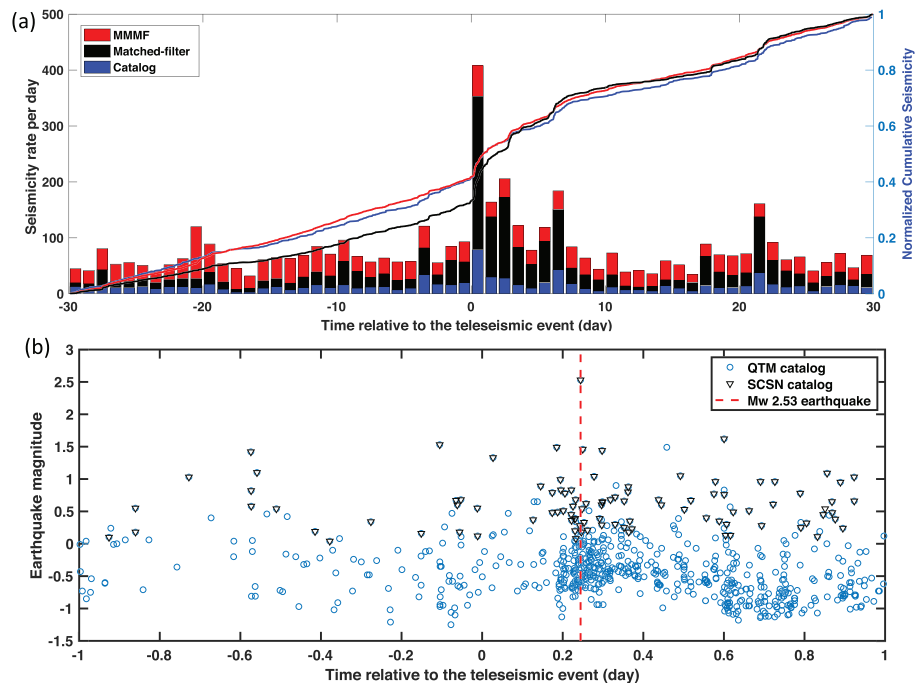
Figure 3. (a) Detection results of local seismicity. The histogram shows the number of detected events, on a daily basis, in the three different catalogs investigated in this study. The lines show the normalized cumulative seismicity, accordingly. (b) Time versus magnitude plot, 1 day before and after the teleseismic event, showing events from the SCSN and QTM catalog (Ross et al., 2019). The dashed red line indicates the largest earthquake (Mw 2.53) in the study region for this time period. MMMF = move max matched-filter; QTM = Quake Template Matching; SCSN = Southern California Seismic Network.

detections (Figure 3a). All three lines in Figure 3a show similar cumulative patterns, yet differ in detail. In the SCSN catalog, there is an ~50% increase in the number of events occurring 1 month after the Papanoa earthquake, while the matched-filter detection results show an ~87% increase in detected events occurring after the Papanoa earthquake during the same period. More interestingly, our MMMF method detects the most events and also shows a ~50% increase in local seismicity as seen in the catalog events, amplifying the detection nearly the same level both before and after the Papanoa earthquake but additionally showing many more detected events in the first 3 days following the mainshock (Figure 3a).

Although the relocated 3,034 local events show an overall similar distribution to that of the catalog events, we note a few significant differences found in detail. The relocated MMMF catalog reveals some linear features along the fault traces (Figure 1b), as well as a sparse area of seismicity between the northwest and southeast earthquake clusters. This less active seismic region is defined as the Anza gap (Rockwell et al., 1990; Sanders & Kanamori, 1984; Thatcher et al., 1975). This gap lies in close proximity to the seismically active triple junction of the Coyote Creek, Clark, and Buck Ridge strands of the SJFZ. A cross section along the SJF trace shows that the earthquake depth distribution is shallow when approaching the Anza gap from the northwest, but then increases in depth when moving away from it towards the southeast (Figure S3).

To investigate the seismicity rate changes in detail, we divide the study region into 0.025° by 0.025° grids and compare their seismic activity 1 month before and after the Mw 7.2 Papanoa earthquake. Figure 1c shows a general seismicity rate increase after the Papanoa earthquake in the study region. Interestingly, new patches of seismicity are observed northwest and southeast of the Anza gap, but no heightened seismicity is observed within the Anza gap itself. In fact, the patch with the highest seismicity rate increase is located ~10 km west of the town of Anza and off the SJF where there are no mapped faults. Since the earthquake cluster shows a planar distribution in 3-D, we determine a best fit plane that has a strike of 215° from north— nearly perpendicular to the strike of the SJF, which is about 306°— and is steeply dipping 83° to the northwest (Figure 4).

4. Discussion

Using the 880 catalog events as templates, the traditional matched-filter method detects 2,835 events, whereas the MMMF detects 4,765 events—approximately 1.7 times that of the matched-filter detections. This result indicates that the MMMF method has a much higher detection capability compared to traditional template matching. We note that the Quake Template Matching (QTM) catalog (Ross et al., 2019), which is created by the template matching method, shows higher earthquake detections (5,934) for the same period. This is because a shorter template window (≤2.5 s for *P* wave templates and 4 s for *S* wave templates) is used, while here, we use a 20-s time window for both *P* and *S* wave templates. This could result in some smaller magnitude events being left out of our catalog since they fell below out pre-set detection thresholds, but for each template event, the MMMF method can detect events within a certain distance range away from the template event, which depends on the allowed time shift (1 s in our case), the velocity model, and station-event distances. Thus, in the QTM catalog, all the earthquakes are in close proximity to the template events (Figure 1b), but our MMMF catalog shows earthquakes distributed over a broader area relative to the template location. Despite differences in the methodology used to derive the QTM and MMMF catalogs, the fault traces delineated are fairly similar. As shown in Figure 1b, both catalogs show seismicity that is spatially distributed around the mapped faults that trend NW-SE. Both catalogs also show that seismicity extends laterally a few kilometers on both sides of the fault traces (Figure 1), down to a depth of 20 km (Figures 4 and S3), with some cross-cutting structures in between. However, at finer scales, it becomes increasingly difficult to interpret new faults traces, especially for small structures where there are limited earthquakes. In the MMMF catalog, we can better capture the unmapped fault by interpreting a broader plane (Figure 4). The MMMF method is also more computationally efficient than the traditional template matching method, especially for large catalogs. It does not require all events recorded in the catalog to be used as templates, as opposed to traditional template matching methods. The study region can be divided into many grid areas based on earthquake distribution for further analyses. When allowing the cross-correlation coefficients to move up to certain time steps, only a few template events—depending on the complexity of local structures and similarity of the waveforms—are needed to capture nearly any missing event in a given grid area.
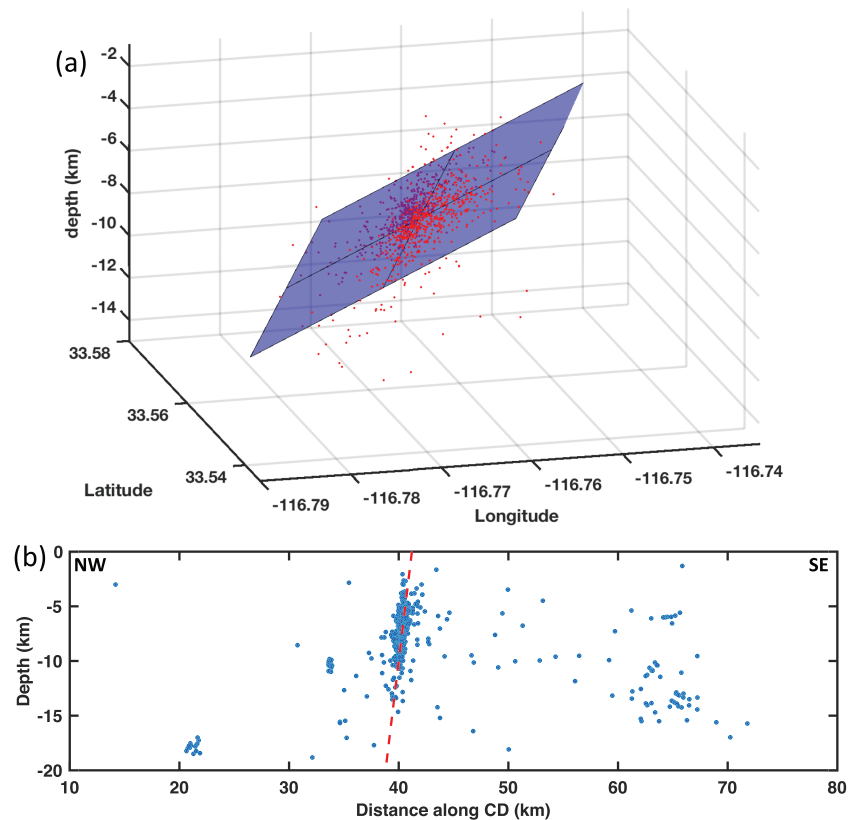
Figure 4. (a) Best fitting fault plane (strike 215°, dip 83°) for the 1,106 relocated earthquakes (red dots) cluster in the red ellipse of Figure 1c. (b) Cross section along the Line C–D, which is perpendicular to the strike of the best fit plane (Table S3). Earthquakes in the yellow polygon (Figure 1b) are plotted. The red dashed line marks the dip of the best fit plane. The cross section is true scale, and plotted below mean sea level.

The seismicity rate changes nonuniformly in the study region, with the most significant patch of seismicity about 10 km west of the SJF and near the town of Anza. Figure 4 shows the 3-D distribution of the relocated earthquakes in this small region, defining a planar structure between depths of 3.5 to 11.5 km that is perpendicular to the SJF. A best fit plane for these locations shows a strike of 215° that is nearly perpendicular to the SJF (306°) and dips steeply at 83° to the northwest (Figure 4). The focal mechanisms of the three largest magnitude (SCSN catalog) earthquakes (Mw 2.53, 1.73, and 2.13) within this patch indicate a normal fault with a strike also perpendicular to the SJF and is steeply dipping (Table S3). This unmapped fault could be the result of the extensional stress from the right lateral San Jacinto and Elsinore fault. A fault of this length (~2.5 km) and width (~8 km) could produce an earthquake up to magnitude 5.3 (Wells & Coppersmith, 1994).

We next investigate the events on this blind fault area recorded in the SCSN catalog for the past 17 years (1 January 2001 to 30 December 2017). We find very little and sparsely distributed seismicity recorded in the catalog before the Papanoa earthquake, implying that this fault has been in a state of seismic quiescence. This quiescence may be due to low tectonic shear stress loading it, since it is nearly perpendicular to the overall kinematic motion of the plate boundary in this region. In addition, the magnitude evolution plot (Figure 3b) using data from the SCSN and QTM catalog (Ross et al., 2019) shows the largest magnitude event in this small region to be a Mw 2.53 that occurred ~5.86 hr after the teleseismic event. In other words, it occurred after the initiation of heightened seismicity with smaller magnitudes and demonstrates that this delayed triggering instance is not a classic example of a mainshock-aftershock sequence. Because this fault did not produce a similar burst of seismicity in the last 17 years, we infer that the burst of seismicity observed in this region is likely delayed triggered caused by the Mw 7.2 Papanoa earthquake and unlikely to be a random (background) occurrence.

This unmapped fault does not seem to extend long enough in its strike direction and is ~10 and ~35 km away from the SJFZ and the Elsinore Fault Zone, respectively. Thus, it limits the likelihood of a through-going rupture from one fault zone to the other (Harris & Day, 1993; Oglesby, 2005), which could increase the potential for a large earthquake in this region. However, it is also possible that the fault could be larger, but only a section of it is active during the time period of this study. In addition, this newly observed normal fault is in close proximity to the Anza gap, an area that has the potential to produce a Mw 6.5 or larger earthquake in the near future (Sanders & Kanamori, 1984; Thatcher et al., 1975). If a large enough earthquake were to occur in the Anza gap, it could trigger earthquakes on this unmapped fault and increase the seismic hazard in the region. The July 4th, 2019 Mw 6.4 Searles Valley and the July 6th, 2019 Mw 7.1 Ridgecrest earthquakes are a sobering example of the hazards posed by unmapped faults in California (Rollins et al., 2019).

In this study, we do not observe dynamically (instantaneously) triggered earthquakes during the passage of the seismic wave train of the 2014 Papanoa earthquake. Still, ~3.5 hr after the passage of the mainshock coda waves, we observe a burst of small local earthquakes. Prior to the arrival of the teleseismic event, the background seismicity rate in the SCSN, QTM, and MMMF catalog is about 9, 75, and 66.4 events per day, respectively. The seismicity rate increased significantly to 79, 583, and 408 events per day in the following 24 hr after the passage of the teleseismic event (Table S2), with heightened seismicity lasting for about 1 week before returning to ambient seismicity levels. This observation may suggest that dynamic stresses imparted by the passage of teleseismic waves may have invoked a time-dependent advance to failure process or other secondary mechanisms that resulted in delayed triggering (Freed, 2005). In the former, the dynamic stresses can influence a fault's earthquake cycle by time advancing it to failure. In other words, faults closer to failure will advance further in time to failure, than faults further away in time from failure (Gomberg et al., 2001; Mendoza et al., 2016). In a population of faults, there will usually be a small fraction of them that are exceptionally close to failure, whereupon the addition of any small stress perturbation can lead to the occurrence of brittle failure (Brodsky & van der Elst, 2014; Gomberg et al., 1998). One proposed mechanism that supports this, is the subcritical crack growth model, which suggests that the intensity of stress at the crack tip (proportional to crack size) controls the rate of crack growth — i.e. earthquake nucleation (Atkinson, 1984). The crack extends very slowly at the start, but when there is a sudden increase in stress at the crack tip, the crack quickly grows, thus leading to what is an apparent delayed fault rupture (Atkinson, 1984; Rinne, 2008). For the seismicity in the unmapped fault region, we observe that the time interval between two consecutive events decreases until there is a burst of seismicity (Figure S4a). In addition, the area of seismicity on this blind fault extends from southwest to northeast and may suggest growth of this fault (Figures 4b and 4c).

Another possible mechanism for delayed triggering in this region could be the enhancement of permeability and subsequent increase in pore pressure due to the oscillatory stresses initiated by teleseismic waves. When the dilatation component of compressional waves interacts with fluids in the crust, it can rupture fluid seals within the fault, unclog fractures, remove temporary barriers, and produce subsequent fluid flow leading to an increase in pore pressure (Brodsky & van der Elst, 2014; Hill et al., 1993). Previous studies show that permeability enhancement increases with amplitude of the seismic waves in Pinon Flat, California, and sustained water level changes at Long Valley Caldera, California, are associated with remote earthquakes up to several thousand miles away (Brodsky et al., 2003; Elkhoury et al., 2006; Roeloffs et al., 2003).

An alternative class of mechanisms to explain the delayed triggering phenomenon in the San Jacinto fault region is that the Papanoa earthquake may have first triggered a local creep or slow slip event (SSE) that then triggered nearby local earthquakes. Using seismic and geodetic data, Wdowinski (2009) proposed that deep creep causes excess seismicity along the San Jacinto fault. Shelly et al. (2011) show that fault creep and triggered tremor initiated by remote earthquakes can last for several days after the passage of teleseismic waves, resulting in a prolonged increase of local seismicity. Other studies have shown that SSEs can trigger both small and large earthquakes and sustain this process as the SSE evolves in space and time (Delahaye et al., 2009; Gomberg et al., 2012; Kato et al., 2012; Peng & Gomberg, 2010; Vidale et al., 2011). Radiguet et al. (2016) infer that an SSE in Guerrero, Mexico, triggered the 2014 Mw 7.2 Papanoa earthquake. Unfortunately, nearby strainmeter stations are unable to identify evidence of fault creep or SSE in the region during this period of elevated seismicity. This may be because stations are not close enough —especially to the most activated unmapped fault area— or perhaps slip is too small to be detectable. Still, recent studies

have identified tectonic tremors in the study region (Hutchison & Ghosh, 2017; Wang et al., 2013). Even though there are observations that SSEs and tremors occur independently (Delahaye et al., 2009; Hutchison & Ghosh, 2016; Li & Ghosh, 2017), generally, they are associated with each other and are known as episodic tremor and slip (Ghosh et al., 2012, 2015; Ito et al., 2007). Tremors and slow slip are most likely the result of the same physical processes along the fault plane (e.g., Ghosh et al., 2012). Thus, a triggered SSE or fault creep in the study region may be responsible for the delayed and sustained increase of seismicity around the SJF. Nonetheless, it is difficult to determine which mechanisms, and to what extent, are driving delayed triggering in the study region.

5. Conclusions

In this study, we use the MMMF method to capture delayed triggering of small local earthquakes in the SJFZ near the Anza Gap in California. The MMMF method detects about 5.4 times the amount of local seismicity found in the SCSN catalogs and 1.7 times the amount of seismicity identified by the traditional matched-filter method, thus greatly improving the completeness of the current earthquake catalog. Although there is no observation of dynamically triggered events during the passage of the teleseismic surface waves, we find a significant increase in the seismicity rate that begins a few hours after the coda and persists for about 1 week, before decaying back down to the background seismicity level. More than one triggering mechanism could be responsible for these observations. They include, but are not limited to: (1) dynamic stresses initiating a time-dependent, advance to brittle failure process, (2) a transient increase in pore pressure, or (3) secondary mechanisms such as fault creep or a SSE. Relocations of seismicity detected by the MMMF method show several linear clusters of seismicity occurring along the SJF system and reveal depth variation, where seismicity is shallow northwest of the Anza gap, and then become increasingly deep as the locations migrate to the southeast. Lastly, a highly active cluster of triggered seismicity implies the existence of an unmapped blind fault that is trending nearly perpendicular (and in close proximity) to the SJF. This blind fault is located ~10 km west of the Anza gap and the town of Anza. If coseismically triggered, it may contribute to the high seismic hazard already posed by the southern San Andreas fault where a large earthquake is overdue.

References

Atkinson, B. K. (1984). Subcritical crack growth in geological materials. *Journal of Geophysical Research*, *89*(B6), 4077–4114. https://doi.org/10.1029/JB089iB06p04077

Bailey, I. W., Ben-Zion, Y., Becker, T. W., & Holschneider, M. (2010). Quantifying focal mechanism heterogeneity for fault zones in central and southern California. *Geophysical Journal International*, *183*(1), 433–450. https://doi.org/10.1111/j.1365-246X.2010.04745.x

Brodsky, E. E., Roeloffs, E., Woodcock, D., Gall, I., & Manga, M. (2003). A mechanism for sustained groundwater pressure changes induced by distant earthquakes. *Journal of Geophysical Research*, *108*(B8), 2390. https://doi.org/10.1029/2002JB002321

Brodsky, E. E., & van der Elst, N. J. (2014). The uses of dynamic earthquake triggering. *Annual Review of Earth and Planetary Sciences*, *42*(1), 317–339. https://doi.org/10.1146/annurev-earth-060313-054648

Delahaye, E. J., Townend, J., Reyners, M. E., & Rogers, G. (2009). Microseismicity but no tremor accompanying slow slip in the Hikurangi subduction zone, New Zealand. *Earth and Planetary Science Letters*, *277*(1-2), 21–28. https://doi.org/10.1016/j.epsl.2008.09.038

Elkhoury, J. E., Brodsky, E. E., & Agnew, D. C. (2006). Seismic waves increase permeability. *Nature*, *441*(7097), 1135–1138. https://doi.org/10.1038/nature04798

Freed, A. M. (2005). Earthquake triggering by static, dynamic, and postseismic stress transfer. *Annual Review of Earth and Planetary Sciences*, *33*(1), 335–367. https://doi.org/10.1146/annurev.earth.33.092203.122505

Ghosh, A., Huesca-Pérez, E., Brodsky, E., & Ito, Y. (2015). Very low frequency earthquakes in Cascadia migrate with tremor. *Geophysical Research Letters*, *42*, 3228–3232. https://doi.org/10.1002/2015GL063286

Ghosh, A., Vidale, J. E., & Creager, K. C. (2012). Tremor asperities in the transition zone control evolution of slow earthquakes. *Journal of Geophysical Research*, *117*, B10301. https://doi.org/10.1029/2012JB009249

Ghosh, A., Vidale, J. E., Peng, Z., Creager, K. C., & Houston, H. (2009). Complex nonvolcanic tremor near Parkfield, California, triggered by the great 2004 Sumatra earthquake. *Journal of Geophysical Research*, *114*, B00A15. https://doi.org/10.1029/2008JB006062

Gibbons, S. J., & Ringdal, F. (2006). The detection of low magnitude seismic events using array-based waveform correlation. *Geophysical Journal International*, *165*(1), 149–166. https://doi.org/10.1111/j.1365-246X.2006.02865.x

Gomberg, J., Beeler, N. M., Blanpied, M. L., & Bodin, P. (1998). Earthquake triggering by transient and static deformations. *Journal of Geophysical Research*, *103*(B10), 24,411–24,426. https://doi.org/10.1029/98JB01125

Gomberg, J., Creager, K., Sweet, J., Vidale, J., Ghosh, A., & Hotovec, A. (2012). Earthquake spectra and near-source attenuation in the Cascadia subduction zone. *Journal of Geophysical Research*, *117*, B05312. https://doi.org/10.1029/2011JB009055

Gomberg, J., Reasenberg, P. A., Bodin, P. L., & Harris, R. A. (2001). Earthquake triggering by seismic waves following the Landers and Hector Mine earthquakes. *Nature*, *411*(6836), 462–466. https://doi.org/10.1038/35078053

Harris, R. A., & Day, S. M. (1993). Dynamics of fault interaction: Parallel strike-slip faults. *Journal of Geophysical Research*, *98*(B3), 4461–4472. https://doi.org/10.1029/92JB02272

Hauksson, E., Yang, W., & Shearer, P. M. (2012). Waveform relocated earthquake catalog for southern California (1981 to June 2011). *Bulletin of the Seismological Society of America*, *102*(5), 2239–2244. https://doi.org/10.1785/0120120010

Hill, D. P., Reasenberg, P. A., Michael, A., Arabaz, W. J., Beroza, G., Brumbaugh, D. S., et al. (1993). Seismicity remotely triggered by the magnitude 7.3 Landers, California, earthquake. *Science*, *260*(5114), 1617–1623. https://doi.org/10.1126/science.260.5114.1617

Hutchison, A. A., & Ghosh, A. (2016). Very low frequency earthquakes spatiotemporally asynchronous with strong tremor during the 2014 episodic tremor and slip event in Cascadia. *Geophysical Research Letters*, *43*, 6876–6882. https://doi.org/10.1002/2016GL069750

Hutchison, A. A., & Ghosh, A. (2017). Ambient tectonic tremor in the San Jacinto Fault, near the Anza Gap, detected by multiple mini seismic arrays. *Bulletin of the Seismological Society of America*, *107*, 1985–1993. https://doi.org/10.1785/0120160385

Ito, Y., Obara, K., Shiomi, K., Sekine, S., & Hirose, H. (2007). Slow earthquakes coincident with episodic tremors and slow slip events. *Science*, *315*(5811), 503–506. https://doi.org/10.1126/science.1134454

Johnson, C. W., Bürgmann, R., & Pollitz, F. F. (2015). Rare dynamic triggering of remote $M \geq 5.5$ earthquakes from global catalog analysis. *Journal of Geophysical Research: Solid Earth*, *120*, 1748–1761. https://doi.org/10.1002/2014JB011788

Kagan, Y. Y., Jackson, D. D., & Rong, Y. (2006). A new catalog of southern California earthquakes, 1800–2005. *Seismological Research Letters*, *77*(1), 30–38. https://doi.org/10.1785/gssrl.77.1.30

Kato, A., Obara, K., Igarashi, T., Tsuruoka, H., Nakagawa, S., & Hirata, N. (2012). Propagation of slow slip leading up to the 2011 Mw 9.0 Tohoku-Oki earthquake. *Science*, *335*(6069), 705–708. https://doi.org/10.1126/science.1215141

Klein, F. W. (2002). User's guide to HYPOINVERSE-2000, a Fortran program to solve for earthquake locations and magnitudes. Open-File Report. https://doi.org/10.3133/ofr02171

Li, B., & Ghosh, A. (2017). Near-continuous tremor and low frequency earthquake (LFE) activities in the Alaska-Aleutian subduction zone revealed by a mini seismic array. *Geophysical Research Letters*, *44*, 5427. https://doi.org/10.1002/2016GL072088

Mendoza, C., & López, M. M. (2017). The Mw 7.3 Papanoa, Mexico earthquake of April18, 2014: Implications for recurrent M > 7 thrust earthquakes in western Guerrero. *Geofisica Internacional*, *56*(1), 13–26.

Mendoza, M. M., Ghosh, A., & Rai, S. S. (2016). Dynamic triggering of small local earthquakes in the central Himalaya. *Geophysical Research Letters*, *43*, 9581–9587. https://doi.org/10.1002/2016GL069969

Meng, X., & Peng, Z. (2014). Seismicity rate changes in the Salton Sea Geothermal Field and the San Jacinto Fault Zone after the 2010 M_w 7.2 El Mayor-Cucapah earthquake. *Geophysical Journal International*, *197*(3), 1750–1762. https://doi.org/10.1093/gji/ggu085

Oglesby, D. D. (2005). The dynamics of strike-slip step-overs with linking dip-slip faults. *Bulletin of the Seismological Society of America*, *95*(5), 1604–1622. https://doi.org/10.1785/0120050058

Peng, Z., & Gomberg, J. (2010). An integrated perspective of the continuum between earthquakes and slow-slip phenomena. *Nature Geoscience*, *3*(9), 599–607. https://doi.org/10.1038/ngeo940

Prejean, S. G., & Hill, D. P. (2009). Earthquakes, dynamic triggering of. In *Encyclopedia of Complexity and Systems Science* (pp. 2600–2621). https://doi.org/10.1007/978-0-387-30440-3_157.

Radiguet, M., Perfettini, H., Cotte, N., Gualandi, A., Valette, B., Kostoglodov, V., & Campillo, M. (2016). Triggering of the 2014 M_w 7.3 Papanoa earthquake by a slow slip event in Guerrero, Mexico. *Nature Geoscience*, *9*(11), 829–833. https://doi.org/10.1038/ngeo2817

Rinne, M. (2008). *Fracture mechanics and subcritical crack growth approach to model time-dependent failure in brittle rock*. Helsinki: Helsinki University of Technology.

Rockwell, T., Loughman, C., & Merifield, P. (1990). Late Quaternary rate of slip along the San Jacinto fault zone near Anza, southern California. *Journal of Geophysical Research*, *95*(B6), 8593–8605. https://doi.org/10.1029/JB095iB06p08593

Roeloffs, E., Sneed, M., Galloway, D. L., Sorey, M. L., Farrar, C. D., Howle, J. F., & Hughes, J. (2003). Water-level changes induced by local and distant earthquakes at Long Valley caldera, California. *Journal of Volcanology and Geothermal Research*, *127*(3-4), 269–303. https://doi.org/10.1016/S0377-0273(03)00173-2

Rollins, C., Stein, R. S., Lin, G., & Kilb, D. (2019). The Ridgecrest earthquakes: Torn ground, nested foreshocks, *Garlock Shocks, and Temblor's Forecast, Temblor*. https://doi.org/10.32858/temblor.039

Ross, Z. E., Trugman, D. T., Hauksson, E., & Shearer, P. M. (2019). Searching for hidden earthquakes in Southern California. *Science*, *364*(6442), 767–771. https://doi.org/10.1126/science.aaw6888

Sanders, C. O., & Kanamori, H. (1984). A seismotectonic analysis of the Anza seismic gap, San Jacinto fault zone, southern California. *Journal of Geophysical Research*, *89*(B7), 5873–5890. https://doi.org/10.1029/JB089iB07p05873

Scott, J. S., Masters, T. G., & Vernon, F. L. (1994). 3-D velocity structure of the San Jacinto fault zone near Anza, California—I. P waves. *Geophysical Journal International*, *119*(2), 611–626. https://doi.org/10.1111/j.1365-246X.1994.tb00145.x

Senobari, N. S., Funning, G. J., Keogh, E., Zhu, Y., Yeh, C. M., Zimmerman, Z., & Mueen, A. (2018). Super-Efficient Cross-Correlation (SEC-C): A Fast Matched Filtering Code Suitable for Desktop Computers. *Seismological Research Letters*, *90*(1), 322–334. https://doi.org/10.1785/0220180122

Shelly, D. R., Beroza, G. C., & Ide, S. (2007). Non-volcanic tremor and low-frequency earthquake swarms. *Nature*, *446*(7133), 305–307. https://doi.org/10.1038/nature05666

Shelly, D. R., Peng, Z., Hill, D. P., & Aiken, C. (2011). Triggered creep as a possible mechanism for delayed dynamic triggering of tremor and earthquakes. *Nature Geoscience*, *4*(6), 384–388. https://doi.org/10.1038/ngeo1141

Thatcher, W., Hileman, J. A., & Hanks, T. C. (1975). Seismic slip distribution along the San Jacinto fault zone, southern California, and its implications. *Geological Society of America Bulletin*, *86*(8), 1140–1146. https://doi.org/10.1130/0016-7606(1975)86<1140:SSDATS>2.0.CO;2

Vidale, J. E., Hotovec, A. J., Ghosh, A., Creager, K. C., & Gomberg, J. (2011). Tiny intraplate earthquakes triggered by nearby episodic tremor and slip in Cascadia. *Geochemistry, Geophysics, Geosystems*, *12*, Q06005. https://doi.org/10.1029/2011GC003559

Waldhauser, F. (2001). hypoDD—A program to compute double-difference hypocenter locations (hypoDD version 1.0-03/2001). *US Geol. Surv. Open File Rep., 01*, 113.

Wang, T. H., Cochran, E. S., Agnew, D., & Oglesby, D. D. (2013). Infrequent triggering of tremor along the San Jacinto fault near Anza, California. *Bulletin of the Seismological Society of America*, *103*(4), 2482–2497. https://doi.org/10.1785/0120120284

Wdowinski, S. (2009). Deep creep as a cause for the excess seismicity along the San Jacinto fault. *Nature Geoscience*, *2*(12), 882–885. https://doi.org/10.1038/ngeo684

Wells, D. L., & Coppersmith, K. J. (1994). New empirical relationships among magnitude, rupture length, rupture width, rupture area, and surface displacement. *Bulletin of the Seismological Society of America*, *84*(4), 974–1002.

Wessel, P., Smith, W. H., Scharroo, R., Luis, J., & Wobbe, F. (2013). Generic mapping tools: Improved version released. *Eos, Transactions American Geophysical Union*, *94*(45), 409–410. https://doi.org/10.1002/2013EO450001

Zhang, M., & Wen, L. (2015). An effective method for small event detection: Match and locate (M&L). *Geophysical Journal International*, *200*(3), 1523–1537. https://doi.org/10.1093/gji/ggu466